University of Nebraska - Lincoln

DigitalCommons@University of Nebraska - Lincoln

2019

High energy product of MnBi by field annealing and Sn alloying

Wenyong Zhang

Balamurugan Balasubramanian

Parashu Kharel

Rabindra Pahari

Shah R. Valloppilly

See next page for additional authors

Authors

Wenyong Zhang, Balamurugan Balasubramanian, Parashu Kharel, Rabindra Pahari, Shah R. Valloppilly, Xingzhong Li, Lanping Yue, Ralph Skomski, and David J. Sellmyer

High energy product of MnBi by field annealing and Sn alloying EP

Wenyong Zhang,[1,2,a] iD   **Balamurugan Balasubramanian,**[1,2] iD   **Parashu Kharel,**[1,3] iD   **Rabindra Pahari,**[1,2] iD
Shah R. Valloppilly,[1] iD   **Xingzhong Li,**[1] iD   **Lanping Yue,**[1]   **Ralph Skomski,**[1,2] iD   and   **David J. Sellmyer**[1,2] iD

AFFILIATIONS

[1] Nebraska Center for Materials and Nanoscience, University of Nebraska, Lincoln, Nebraska 68588, USA
[2] Department of Physics and Astronomy, University of Nebraska, Lincoln, Nebraska 68588, USA
[3] Department of Physics, South Dakota State University, Brookings, South Dakota 57007, USA

[a] E-mail: wenyong.zhang@unl.edu

ABSTRACT

Permanent-magnet materials are one cornerstone of today's technology, abundant in disk drives, motors, medical equipment, wind generators, and cars. A continuing challenge has been to reconcile high permanent-magnet performance with low raw-material costs. This work reports a Mn-Bi-Sn alloy exclusively made from inexpensive elements, exhibiting high values of Curie-temperature, magnetization, anisotropy, coercivity, and energy product. The samples are produced by field annealing of rapidly quenched Sn-containing MnBi alloys, where the improvement of the magnetic properties is caused by the substitutional occupancy of the 2c sites in the hexagonal NiAs structure by Sn. The substitution modifies the electronic structure of the compound and enhances the magnetocrystalline anisotropy, thereby improving the coercivity of the compound. The energy product reaches 114 kJ/m^3 (14.3 MGOe) at room temperature and 86 kJ/m^3 (10.8 MGOe) at $200\,°$C; this value is similar to that of the Dy-free $Nd_2Fe_{14}B$ and exceeds that of other rare-earth-free permanent-magnet bulk alloys, as encountered in automotive applications.

Permanent magnets require not only a high saturation magnetization M_s and a high Curie temperature T_c but also a high coercivity H_c.[1–8] Magnetization and coercivity largely determine the energy product $(BH)_{max}$ of a permanent magnet, a key figure of merit that describes the magnet's ability to store magnetostatic energy in free space.[8] While the energy product never exceeds $J_s{}^2/4$ ($J_s = \mu_0 M_s$ is the saturation magnetic polarization), the main limitation is usually the coercivity. A key question is therefore the improvement of coercivity by enhancing the magnetocrystalline anisotropy and by creating a microstructure that prevents magnetization reversal in small reverse magnetic fields.[9] It is relatively easy to ensure appreciable magnetizations and Curie temperature by using 3d elements such as Fe and Co, but high anisotropies tend to require expensive and/or supply-threatened elements such as rare earths and Pt.[8,10–12] Cobalt, used, for example, in $SmCo_5$,[10,11] is a special case: it is more expensive than Fe or Mn and exhibits industrially disadvantageous price fluctuations. Today's leading

room-temperature high-performance permanent magnets are made from the fairly expensive alloy $Nd_2Fe_{14}B$.[8,12,13] Furthermore, powerful Nd-Fe-B motors, for example, in automotive applications, operate at temperatures of up to $200\,°$C. The anisotropy of $Nd_2Fe_{14}B$ strongly decreases with increasing temperature, which is compensated by the addition of Dy, an expensive rare-earth element.[3,4,14–16]

MnBi was discovered in 1904 as a by-product of the original research on Heusler alloys[17] and later shown to crystallize in the hexagonal NiAs structure (space group $P6_3/mmc$), as shown in Fig. 1.[18] Alongside other rare-earth-free materials,[3,19–24] MnBi has long been considered as a potential permanent-magnet material since it contains neither rare earths nor expensive elements such as Ga and Pt. The magnetic-ordering temperature of MnBi, $377\,°$C, is higher than that of $Nd_2Fe_{14}B$ ($312\,°$C), the saturation magnetic polarization of $J_s \approx 0.85$ T is appreciable,[3,9] and its anisotropy exhibits the unusual advantage of increasing with temperature.[25–28]
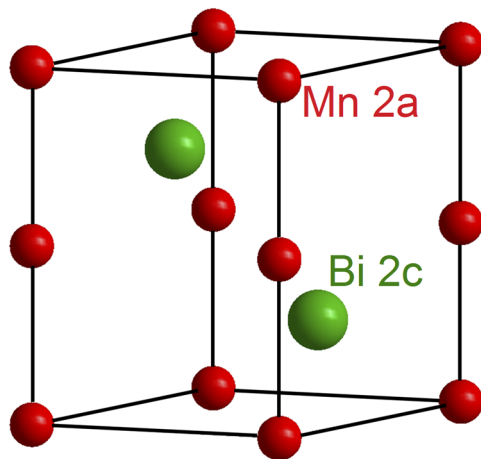
FIG. 1. A schematic of the unit cell of MnBi.

However, the structure of MnBi is nontrivial, the ordering or Curie temperature actually is being a phase-transformation from a low-temperature phase (LTP) to a high-temperature phase (HTP),[29] and its room-temperature magnetocrystalline anisotropy of 1.2 MJ/m^3 is relatively low.

Based on density-functional calculations, Sakuma et al. suggested that the addition of Sn improves the anisotropy of MnBi.[30] In their calculation, Sn occupies the 2c sites in the NiAs structure (Fig. 1), in agreement with the experimental situation in alloys of iron-series transition-metals and heavy metalloids.[31,32] While Bi and Sn are nonmagnetic, they affect the magnetic anisotropy of the Mn sublattice through crystal-field or "ligand-field" interactions.[8,33] In the present system, there is a shift of the Fermi level to lower energies because Sn has one fewer valence electrons than Bi. This yields a slight reduction in magnetization and Mn-Mn interatomic exchange, but an enhancement of the first anisotropy constant K_1.[30]

In our experiments, we have focused on simultaneously improving the anisotropy, coercivity, and energy product of MnBi. The anisotropy is modified by Sn addition and supplemented by optimizing the microstructure through annealing in high magnetic fields. Empirical annealing procedures, which are common in permanent-magnet processing, have multiple purposes and require material-specific adjustments. In the present case, they control the complicated microchemistry of MnBi,[33] improve the grain alignment to enhance the remanent magnetization, and optimize the grain-boundary morphology. We have used melt spinning to produce rapidly quenched ribbons of approximate dimensions 100 μm (thickness), 2 mm (width), and several centimeters (length). Subsequent annealing at 400 °C was then performed in the zero magnetic field and in the magnetic fields of 1, 2, 3, and 4 T.

We first produced MnBi and MnBi$_{1-x}$Sn$_x$ ingots by arc melting high-purity elements in an argon atmosphere. The ribbons were then prepared by ejecting the induction-melted ingots from a quartz tube onto the surface of a water-cooled copper wheel rotating at a speed of 20 m/s. The rapidly quenched ribbons were annealed at 400 °C for 10 min in a high-field annealing furnace and pumped to a base pressure of 8 × 10^{-8} Torr. The samples were annealed at 0, 1, 2, and 4 T, setting the field direction parallel to the length of the

ribbons. The direction along the ribbon length is therefore expected to be the easy magnetization axis, whereas the hard magnetization axes are the directions perpendicular to the ribbon length, i.e., the directions along the width and thickness (see below). The crystal structure and phase composition in the samples were determined by x-ray diffraction (XRD) using a Rigaku D/Max-B X-ray diffractometer with Co Kα radiation. The TOtal PAttern Solution (TOPAS) software was used to analyze the XRD patterns. The magnetic properties including field-dependent magnetizations $M(H)$ and thermomagnetic curves $M(T)$ were measured using a Quantum Design Physical Property Measurement System (PPMS).

Figure 2(a) shows the out-of-plane x-ray diffraction (XRD) patterns of the MnBi and MnBi$_{0.9}$Sn$_{0.1}$ samples, produced by melt-spinning and annealed at 400 °C in the zero field and in the fields of 2 and 4 T. The patterns (i, iii) of the melt-spun ribbons annealed in the zero field are indexed to the hexagonal NiAs structures, indicating that the annealed samples contain LTP MnBi only. The lattice parameters obtained from the XRD patterns of the zero-field annealed samples, Fig. 2(b), are $a = 4.286$ Å and $c = 6.122$ Å for MnBi and $a = 4.284$ Å and $c = 6.119$ Å for MnBi$_{0.9}$Sn$_{0.1}$. Our MnBi lattice parameters are close to those previously reported for LTP MnBi,[34] and the small decrease in lattice parameters for the Sn doped samples reflects the smaller atomic radius of Sn compared to Bi. The field annealing does not change the lattice parameters but leads to the development of a strong texture in the samples, as evidenced by the disappearance of (002) and (004) peaks and strong (110) peaks in the curves (ii, iv, and v) in Fig. 2(a). This, along with magnetization data for B along the ribbon length and the directions perpendicular to the ribbon length, along the width and thickness of the ribbons (not shown here), suggests that the crystallographic c-axis of the MnBi grains is parallel to the length of the ribbons. We have also carried out tilt-angle x-ray diffraction measurements, and the data clearly demonstrate that a significant grain reorientation is achieved with the c-axis aligned nearly parallel to the ribbon plane (along the length of the ribbon), within 10°–15° from the surface (Fig. S1 of the supplementary material).

We have used the Williamson Hall method to determine the crystallite size and microstrain in the annealed samples (Fig. S2 of
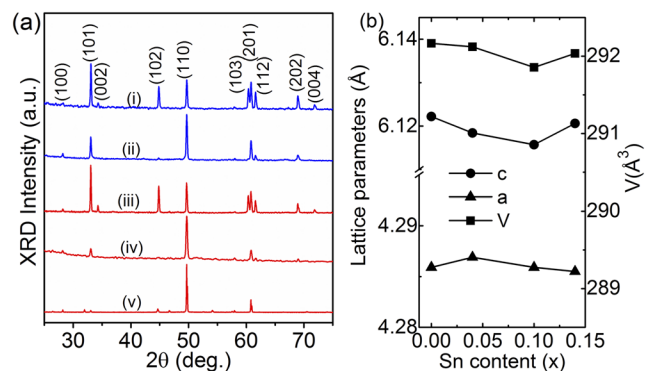

FIG. 2. Structure of MnBi(Sn): (a) X-ray diffraction (XRD) patterns of the zero-field annealed MnBi (i) and MnBi$_{0.9}$Sn$_{0.1}$ (iii) and field-annealed MnBi at 2 T (ii) and MnBi$_{0.9}$Sn$_{0.1}$ at 2 T (iv) and 4 T (v) and (b) Sn-content dependence of lattice parameters and cell volume (V) for the zero-field annealed samples.

the supplementary material). This analysis yields negligibly small microstrain (≤0.04%) in the annealed MnBi and Sn-substituted MnBi samples. The average crystallite sizes are determined as 59 ± 7 nm (MnBi) and 62 ± 4 nm ($MnBi_{0.9}Sn_{0.1}$) for the annealed samples in the zero field. The crystallite-size values for the annealed samples in the magnetic field are 44 ± 2 nm (MnBi) and 42 ± 5 nm ($MnBi_{0.9}Sn_{0.1}$), and the result shows a reduction of about 30% crystallite size upon field annealing.

Figure 3(a) shows the temperature dependences of the magnetic polarization, $J = \mu_0 M$, for the MnBi and $MnBi_{0.9}Sn_{0.1}$ ribbons annealed at 2 T and measured in a field $B_0 = \mu_0 H = 0.1$ T applied along the ribbon length. The $J(T)$ curves show two clear transitions, a low-temperature spin-reorientation transition where the easy magnetization axis flips from the basal plane (a-b plane) to the c-axis[35] and a high-temperature structural transition from ferromagnetic LTP MnBi to the paramagnetic HTP MnBi.[36] The dJ/dT curves, Fig. 3(b), show that the temperatures of the spin-reorientation transition (T_{sr}) and of the structural transition (T_c) slightly decrease on Sn doping. The slight decrease in T_c due to Sn doping is consistent with the theoretical predictions by Sakuma et al.[30]

Figures 4(a) and 4(b) show the hysteresis loops of the field-annealed samples measured at room temperature (a) and at 200 °C (b) along the easy-axis direction (the measurement field being applied along the ribbon length). We find that the saturation magnetic polarization J_s of the Sn-doped ribbons is slightly lower than that of pure MnBi at 300 K (Fig. S3 of the supplementary material), which agrees with the theoretical predictions.[30] However, this effect is overcompensated by the enhanced remanence J_r, as evidenced by the improved loop squareness of the Sn-doped samples (Fig. S4 of the supplementary material). The remanence ratios J_r/J_s of both MnBi and $MnBi_{0.9}Sn_{0.1}$ ribbons systematically increase with the annealing field, reaching almost 1 for the annealing field of 4 T (not shown here).

Figure 4(c) plots the room-temperature coercivity ($B_c = \mu_0 H_c$) and energy product as a function of the annealing field. The coercivities of MnBi and $MnBi_{0.9}Sn_{0.1}$ slightly decrease upon annealing, which probably reflects facilitated domain-wall motion due to grain alignment. The Sn doping enhances the energy product, due to the improved remanence ratio and, at room-temperature, the enhanced coercivity. To determine the first and second order anisotropy constants K_1 and K_2, respectively, we have used the Sucksmith-Thompson plot for the field-dependent room-temperature magnetic
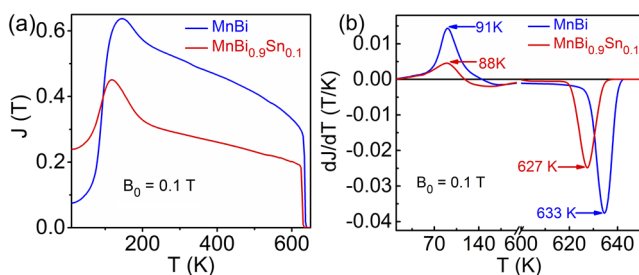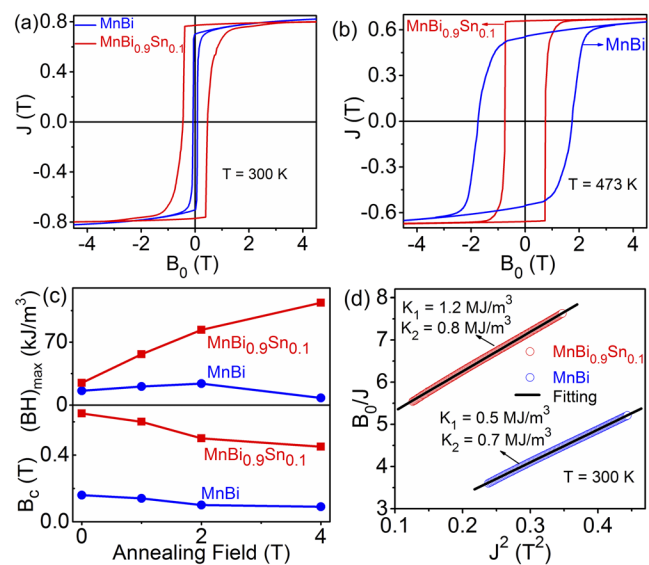

FIG. 4. Magnetic properties of the field-annealed MnBi (blue) and $MnBi_{0.9}Sn_{0.1}$ (red). Hysteresis loops for the annealed samples at 4 T measured at 300 K (a) and 473 K (b). The room-temperature coercivity and energy product as a function of the annealing field (c) and Sucksmith-Thomson plots at 300 K for the samples annealed at 4 T (d).

polarization curves measured along the hard axis (the measurement field being applied along the width of the ribbon).[37,38] The method analyzes B_0/J as a function of J^2 and yields the fit of Fig. 4(d). The values of $K = K_1 + K_2$ are 1.2 MJ/m³ and 2.0 MJ/m³ at room temperature for MnBi and $MnBi_{0.9}Sn_{0.1}$, respectively.

The room-temperature coercivity of $MnBi_{0.9}Sn_{0.1}$ is significantly higher than that of MnBi, which is consistent with the increase in K measured for $MnBi_{0.9}Sn_{0.1}$ in the present study and theoretically predicted enhancement of the magnetocrystalline anisotropy.[30] However, microstructural changes caused by annealing, such as grain-size refinement shown by XRD analysis and a possible pinning mechanism at grain boundaries, may also play a role in improving the coercivities in the Sn-substituted samples. Therefore, it is likely that the enhanced coercivity in $MnBi_{0.9}Sn_{0.1}$ reflects the increase in anisotropy, complemented by microstructural refinement through annealing. At 200 °C, the effect of Sn lowers the coercivity because the thermal effect was not considered by Sakuma et al.[30] However, the energy product remains high because of good loop squareness.

The maximum room-temperature energy product $(BH)_{max}$ is equal to 114 kJ/m³ for the $MnBi_{0.9}Sn_{0.1}$ sample annealed at 4 T, compared to 67 kJ/m³ previously achieved in microcrystalline MnBi.[16,23] High-performance permanent-magnet materials are usually defined by energy products in excess of 100 kJ/m³.[8,9] Various types of Sm-Co and Nd-Fe-B magnets clearly exceed this threshold (see, e.g., Table A 4 in Ref. 9), but they contain expensive elements. Room-temperature MnBi energy products as high as 130 kJ/m³ have been achieved in textured thin films of MnBi on glass substrates,[39] but these structures are generally not suitable for industrial applications. By contrast, melt spinning can be realized on an industrial scale, as exemplified by bonded $Nd_2Fe_{14}B$ magnets. At 200 °C, the energy product

FIG. 3. Temperature dependence of the magnetic polarization of MnBi and $MnBi_{0.9}Sn_{0.1}$ annealed at 2 T: (a) $J(T)$ and (b) dJ/dT. The spin-reorientation and Curie temperatures are nearly 90 K and 630 K, respectively.

of $MnBi_{0.9}Sn_{0.1}$ is 86 kJ/m^3, similar to that of Dy-free $Nd_2Fe_{14}B$ and higher than that of other rare-earth-free bulk alloys.[16]

There are two reasons for the present improvement, namely, the high volume fraction of the hard phase (no grain boundary phase) and the better c-axis alignment of the grains. Previously investigated MnBi-based magnets are nearly isotropic and exhibit lower coercivities and energy products.[16,23,26,40] The formation of a Bi grain boundary phase, which helps to develop coercivity, also limits the energy product because Bi is nonmagnetic.[19] By comparison, Sn replaces Bi in MnBi and does not therefore significantly reduce magnetization. Recent research on alloying MnBi with elements including Sn,[41] Sb, and Mg[42–44] has been shown to increase the coercivity and energy product. In particular, a maximum energy product of 92 kJ/m^3 has been obtained in a compacted magnet with a nominal composition of $Mn_{50}Bi_{46.5}Mg_3Sb_{0.5}$.[44] It may also be possible to produce bulk magnets using magnetically aligned $MnBi_{0.9}Sn_{0.1}$ ribbons by following the standard processing method used to fabricate bonded magnets.[26,45] That is, bulk $MnBi_{0.9}Sn_{0.1}$ may be fabricated by crushing the ribbons into micrometer-sized powder, mixing the particles homogeneously using epoxy resin, and solidifying them in a magnetic field of 1–3 T. Such processing studies remain for the future.

In conclusion, we have developed a new processing method and produced MnBi with a high room-temperature energy product of 114 kJ/m^3. The energy-product improvement has been achieved by high-field annealing in combination with Sn substitution for Bi. Our alloy can be regarded as a low-cost high-performance permanent-magnet material for applications that require energy products between mass-produced cheap ferrite magnets and expensive high-performance rare-earth magnets. The melt-spun ribbons may be further processed to create bulk magnets by milling and polymer or metal bonding, similar to bonded ferrite or Nd-Fe-B magnets.

See the supplementary material for the additional figures, analysis, and discussion.

REFERENCES

[1]J. S. Jiang and S. D. Bader, J. Phys.: Condens. Matter **26**, 064214 (2014).

[2]A. K. Pathak, M. Khan, K. A. Gschneidner, Jr., R. W. McCallum, L. Zhou, K. Sun, K. W. Dennis, C. Zhou, K. Sun, K. W. Dennis, C. Zhou, F. E. Pinkerton, M. J. Kramer, and V. K. Pecharsky, Adv. Mater. **27**, 2663 (2015).

[3]J. Cui, M. Kramer, L. Zhou, F. Liu, A. Gabay, G. Hadjipanayis, B. Balasubramanian, and D. J. Sellmyer, Acta Mater. **158**, 118 (2018).

[4]O. Gutfleisch, M. A. Willard, E. Brück, C. H. Chen, S. G. Sankar, and J. P. Liu, Adv. Mater. **23**, 821 (2011).

[5]J. M. D. Coey, IEEE Trans. Magn. **47**, 4671 (2011).

[6]J. M. D. Coey, J. Phys.: Condens. Matter **26**, 064211 (2014).

[7]R. Skomski, P. Manchanda, P. Kumar, B. Balamurugan, A. Kashyap, and D. J. Sellmyer, IEEE Trans. Magn. **49**, 3215 (2013).

[8]R. Skomski and J. M. D. Coey, *Permanent Magnetism* (Institute of Physics, Bristol, 1999).

[9]R. Skomski, J. Phys.: Condens. Matter **15**, R841 (2003).

[10]K. J. Strnat and R. M. W. Strnat, J. Magn. Magn. Mater. **100**, 38 (1991).

[11]K. Kumar, J. Appl. Phys. **63**, R13 (1988).

[12]J. F. Herbst, Rev. Mod. Phys. **63**, 819 (1991).

[13]L. Li, A. Tirado, I. C. Nlebedim, O. Rios, B. Post, V. Kunc, R. R. Lowden, E. Lara-Curzio, R. Fredette, J. Ormerod, T. A. Lograsso, and M. P. Paranthaman, Sci. Rep. **6**, 36212 (2016).

[14]N. Jones, Nature **472**, 22 (2011).

[15]R. G. Eggert, Nat. Chem. **3**, 688 (2011).

[16]R. W. McCallum, L. H. Lewis, R. Skomski, M. J. Kramer, and I. E. Anderson, Annu. Rev. Mater. Res. **44**, 451 (2014).

[17]F. Heusler, Z. Angew. Chem. **17**, 260 (1904).

[18]R. M. Bozorth, *Ferromagnetism* (van Nostrand, Princeton, New Jersey, 1951).

[19]W. Y. Zhang, X. Z. Li, S. Valloppilly, R. Skomski, J. E. Shield, and D. J. Sellmyer, J. Phys. D: Appl. Phys. **46**, 135004 (2013).

[20]B. Balamurugan, B. Das, W. Y. Zhang, R. Skomski, and D. J. Sellmyer, J. Phys.: Condens. Matter **26**, 064204 (2014).

[21]M. A. McGuire, O. Rios, N. J. Ghimire, and M. Koehler, Appl. Phys. Lett. **101**, 202401 (2012).

[22]A. A. El-Gendy and G. Hadjipanayis, J. Phys. D: Appl. Phys. **48**, 125001 (2015).

[23]J. Cui, J. P. Choi, E. Polikarpov, M. E. Bowden, W. Xie, G. S. Li, Z. M. Nie, N. Zarkevich, M. J. Kramer, and D. Johnson, Acta Mater. **79**, 374 (2014).

[24]H. Kronmüller, J. B. Yang, and D. Goll, J. Phys.: Condens. Matter **26**, 064210 (2014).

[25]P. A. Albert and W. J. Carr, J. Appl. Phys. **32**, S201 (1961).

[26]J. B. Yang, Y. B. Yang, X. G. Chen, X. B. Ma, J. Z. Han, Y. C. Yang, S. Guo, A. R. Yan, Q. Z. Huang, M. M. Wu, and D. F. Chen, Appl. Phys. Lett. **99**, 082505 (2011).

[27]X. Guo, X. Chen, Z. Altounian, and J. O. Ström-Olsen, Phys. Rev. B **46**, 14578 (1992).

[28]J. Cui, J.-P. Choi, G. Li, E. Polikarpov, J. Darsell, N. Overman, M. Olszta, D. Schreiber, M. Bowden, T. Droubay, M. J. Kramer, N. A. Zarkevich, L. L. Wang, D. D. Johnson, M. Marinescu, I. Takeuchi, Q. Z. Huang, H. Wu, H. Reeve, N. V. Vuong, and J. Ping Liu, J. Phys.: Condens. Matter **6**, 064212 (2014).

[29]J. B. Goodenough, *Magnetism and the Chemical Bond* (Wiley, New York, 1963).

[30]A. Sakuma, Y. Manabe, and Y. Kota, J. Phys. Soc. Jpn. **82**, 073704 (2013).

[31]M. Ellner, J. Less-Common Met. **48**, 21 (1976).

[32]H. Fjellvag and A. Kjekshus, Acta Chem. Scand. **40**, 23 (1986).

[33]C. J. Ballhausen, *Introduction to Ligand Field Theory* (McGraw-Hill, New York, 1962).

[34]K. Kang, W. S. Yoon, S. Park, A. R. Moodenbaugh, and L. H. Lewis, Adv. Funct. Mater. **19**, 1100 (2009).

[35]B. W. Roberts, Phys. Rev. **104**, 607 (1956).

[36]K. Kang, A. R. Moodenbaugh, and L. H. Lewis, Appl. Phys. Lett. **90**, 153112 (2007).

[37]W. Sucksmith and J. E. Thompson, Proc. Roy. Soc. A **225**, 362 (1954).

[38]M. H. Yu, O. Tegus, Y. Janssen, J. C. P. Klaase, Z. D. Zhang, E. Brück, F. R. de Boer, and K. H. J. Buschow, J. Alloys Compd. **333**, 51 (2002).

[39]W. Y. Zhang, P. Kharel, S. Valloppilly, L. P. Yue, and D. J. Sellmyer, Phys. Status Solidi B **252**, 1934 (2015).

[40]A. M. Gabay, G. C. Hadjipanayis, and J. Cui, AIP Adv. **8**, 056702 (2018).

[41]W. Zhang, R. Skomski, P. R. Kharel, L. Yue, and D. J. Sellmyer, "EI-05. Magnetic property enhancement of high-field-annealed rapidly-quenched MnBi due to Sn addition," in Joint MMM-Intermag Conference, January 14–18, 2019, Washington, DC, 2019.

[42]T. X. Nguyen, H. V. Pham, and V. V. Nguyen, Physica B **552**, 190 (2019).

[43]A. M. Gabay, G. C. Hadjipanayis, and J. Cui, J. Alloys Compd. **792**, 77 (2019).

[44]A. M. Gabay, G. C. Hadjipanayis, and J. Cui, J. Magn. Magn. Mater. **495**, 165860 (2020).

[45]J. B. Yang, W. B. Yelon, W. J. James, Q. Cai, and N. Ali, J. Appl. Phys. **91**, 7866 (2002).